Journal of
Materials Chemistry C

RSC Publishing

PAPER

Cite this: *J. Mater. Chem. C*, 2013, 1, 299

Synthesis and low-potential electrogenerated chemiluminescence of surface passivated phenol formaldehyde resin@CdS quantum dots

Shengyuan Deng, Jianping Lei, Xiaonan Yao, Yin Huang, Dajie Lin and Huangxian Ju*

Received 22nd August 2012
Accepted 2nd October 2012

DOI: 10.1039/c2tc00028h

www.rsc.org/MaterialsC

A novel method for the synthesis of polymer-stabilized quantum dots (QDs) was reported through a one-pot hydrothermal reaction. Using this method, a phenol formaldehyde resin (PFR) polymer was formed *in situ* to passivate the surface of the CdS QDs with hexamethylenetetramine as the source of both the monomer and the crosslinking agent, HCHO. The PFR-capped QDs possessed a uniform size distribution with controllable surface states, and showed a unique electrogenerated chemiluminescent (ECL) spectrum with two peaks at 537 and 573 nm, which corresponded to the core and surface states of the QDs, respectively. The partially unpassivated surface state produced a low-potential ECL emission with a relatively long lifetime at −0.78 V. A new signal tag was thus designed for "signal-on" ECL immunoassay by concentrating QDs on carbon nanospheres to label the signal antibody, realizing the immunodetection of carcinoembryonic antigen. The excellent analytical performance indicated the promising application of the surface passivated PFR-capped QDs in optoelectronic and biomedical devices.

Introduction

Semiconductor nanoparticles, or quantum dots (QDs), have unique photophysical properties, such as size-controlled fluorescence (PL), surface- or core-derived electrogenerated chemiluminescence (ECL), high quantum yields and stability against photobleaching.[1–6] These properties enable the use of QDs as nanoemitting labels for the analysis of immunocomplexes or DNA hybridization processes.[2,3] Although QDs with excitonic luminescence are suitable for ECL study and have been applied in many fields,[7] the QDs-based ECL is sensitive to the surface states by its electro-driven nature and has become an exclusive and powerful tool for probing the surface chemistry and signal transduction,[1] which also makes the surface-derived ECL emission superior to the core-derived type.[8–11] For example, since the surface states generally show narrower band gaps compared with the core,[4,11] they always emit the ECL signal at a longer wavelength and lower potential,[4,8,10] which helps to maintain the bioactivity of detection targets, secure the specificity and exclude the interference from the coexisting electroactive species, whereas the excitonic luminescence usually occurs at a high applying potential. Therefore, although the surface-derived luminescence of QDs is very broad and cannot be easily controlled, their ECL applications favor the surface states. Moreover, the surface-derived ECL emission can produce stronger ECL emission due to the potential electron/hole-injected traps of the unpassivated surface state, making the electron transfer between the surface of the QDs and the coreactant or electrode easier.[9,11] These advantages lead to sensitive low-potential ECL emission.

The QDs-based ECL emission has been confirmed depending on the capping agents.[12,13] To produce the surface-state controlled ECL emission, specific small molecules with rigid structures have been selected to passivate the surface of the QDs, which leads to the formation of surface traps. For example, the steric hindrance from the two *cis*-carboxyl groups of *meso*-2,3-dimercaptosuccinic acid (DMSA) can create a large amount of surface traps on DMSA-CdTe QDs.[14] Another way for intentional introduction of surface traps is using dual ligands such as mercaptopropionic acid (MPA) and sodium hexametaphosphate,[8] and trioctylphosphine oxide (TOPO) and dodecylamine[4] instead of one ligand to passivate the surface of QDs. Hexametaphosphate and dodecylamine can hinder the formation of a well-coated QD shell, leading to a great number of unpassivated traps on the surface of QDs. Although amphiphilic polymers have been used for the modification of QD surfaces by the hydrophobic side chain to interact with the organic capping layer and a polyethylene glycol backbone for water solubility,[15,16] this kind of polymer cannot provide QDs with surface-state controlled ECL emission.

In order to take the advantages of surface-state controlled ECL and extend the application of QDs to bioanalysis, this work developed a novel method for the synthesis of polymer-stabilized CdS QDs by a hydrothermal approach and studied the ECL behaviors of obtained phenol formaldehyde resin (PFR) polymer passivated CdS QDs. The PFR polymer was formed *in situ* to

State Key Laboratory of Analytical Chemistry for Life Science, School of Chemistry and Chemical Engineering, Nanjing University, Nanjing 210093, P.R. China. E-mail: hxju@nju.edu.cn

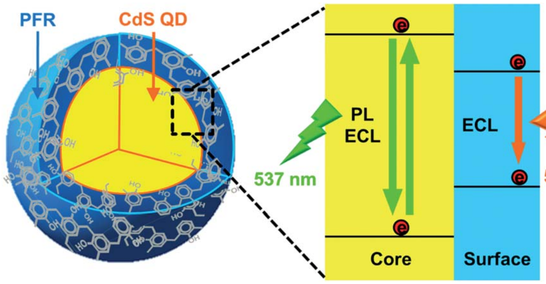

Scheme 1 Schematic illustration of PL and the surface and core ECL mechanisms of PFR-CdS QDs.

passivate the QDs with hexamethylenetetramine (HMTA) as the source of both the monomer and the crosslinking agent (HCHO).[17] The PFR encapsulation led to uniform spatial distribution and partially unpassivated surface of QDs, which produced strong surface-state controlled ECL emission at relatively low potential (Scheme 1). The introduction of surface states elongated the excited lifetime of injected electrons by trapping them at the intrinsic low conduction band. The newly synthesized QDs could be conveniently used to label biorecognition elements such as antibodies, leading to a new "signal-on" probe for a QDs-based ECL immunoassay. The proposed method showed excellent analytical performance, indicating the potential application of the polymer passivated QDs in optoelectronic and biomedical devices.

Experimental

Preparation of the PFR-stabilized CdS QDs

The PFR-CdS QDs were prepared by *in situ* polymerization with HMTA as the source of both the monomer and the crosslinking agent (HCHO), and simultaneous formation of CdS QDs with a hydrothermal method at 160 °C (Scheme 2). Briefly, 40 mL aqueous solution containing 10 mM $CdCl_2$ and 10 mM thioacetamide (TAA) was extensively stirred for 30 min in the ice-water bath. Subsequently, 0.025 mmol phenol and 0.01 mmol HMTA were dissolved in the precursor solution with mild stirring for 30 min. The resulting solution was transferred into a Teflon-lined stainless steel autoclave (50 mL) and heated to 160 °C for 4 h. During the hydrothermal reaction, both TAA and HMTA were decomposed to produce ammonia, which made the initial growth of the CdS nucleus slow. Meanwhile, the produced NH_3 could react with the formed HCHO to give an intermediate of aminomethylated Mannich base for the polymerization.[17,18] The formed PFR-CdS QDs solution was sedimented by adding 1 : 1 (V/V) of ethanol/water overnight. After decanting the supernatant, the sedimented QDs were washed with ethanol and ultrapure water several times to remove inorganic ions and other impurities by centrifugation. Finally, the product was concentrated by ultrafiltration at 5000 *rcf* for 10 min at 4 °C. The obtained QDs solution was kept at 4 °C prior to use. As a control, PFR, CdS QDs without PFR and PFR-CdS QDs with *m*-cresol instead of phenol as the monomer were synthesized following the same route.

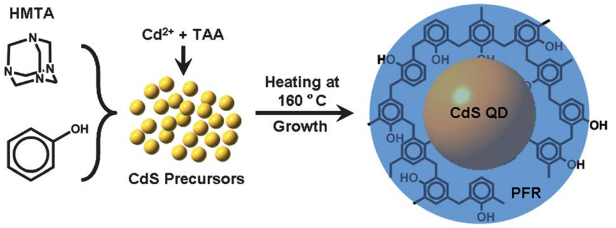

Scheme 2 Schematic illustration of the synthesis of the PFR-CdS QDs.

Preparation of the PFR-CdS QDs labeled tracing tag

Carbon nanospheres (CNSs) were prepared according to the reported method.[19] The as-prepared CNSs were further treated with 3 : 1 H_2SO_4/HNO_3 (V/V) to induce carboxylic groups on the surface by stirring for 4 h, followed by repeated centrifugation and washing until the pH reached 7. Then, 1 mg mL^{-1} of carboxylated CNSs was dispersed in a 0.5% poly(diallyldimethylammonium chloride) (PDDA, M_W 200 000–350 000) aqueous solution containing 0.5 M NaCl by stirring for 30 min to give a homogeneous brown suspension. Residual PDDA was removed by high-speed centrifugation, and the complex was thrice washed with ultrapure water to obtain PDDA-functionalized CNSs (PCNSs).

100 μL of 1 mg mL^{-1} PCNSs was allowed to adsorb QDs by vortexing with 400 μL of 10.3 μM PFR-CdS QDs through electrostatic interaction for 2 h at room temperature. The resulting PFR-CdS QDs@PCNS nanocomposites were centrifuged at 3000 *rcf* for 10 min to remove unbound QDs by decanting the supernatant. The as-prepared PFR-CdS QDs@PCNSs were redispersed in 200 μL of 0.01 M pH 6.0 phosphate buffer saline (PBS) containing 0.5 μg mL^{-1} polyclonal anti-carcinoembryonic antigen (CEA) secondary antibody (Ab_2, clone no. 28E4) and allowed to vortex thrice for 30 min with 30 min intervals and stand overnight at 4 °C, during which the PFR-CdS QDs@PCNSs adsorbed Ab_2 through electrostatic interaction. After shaking for 1 h at room temperature, the mixture was centrifuged twice at 5000 *rcf* at 4 °C for 10 min and washed with PBS to obtain the labeled Ab_2 tag (PFR-CdS QDs@PCNSs/Ab_2), which was redispersed in 100 μL of 0.01 M pH 6.0 PBS for immunoassay.

Preparation of the ECL immunosensor and the immunoassay procedure

20 μL of 0.5% PDDA aqueous solution containing 0.5 M NaCl was dropped on the surface of a glassy carbon electrode (GCE) for 2 h to adsorb positively charged PDDA as a precursor layer at 36 °C. After washing with drips of ultrapure water, 20 μL of 2 mg mL^{-1} reduced L-glutathione (GSH)-stabilized AuNPs, which were prepared based on the reported method,[20] was dropped on the electrode to adsorb the negatively charged GSH-AuNPs and dried at room temperature overnight. For the anti-CEA primary antibody (Ab_1, clone no. 27D6) attachment, 20 μL of freshly prepared 400 mM 1-ethyl-3-(3-dimethylaminopropyl) carbodiimide (EDC) and 100 mM *N*-hydroxysulfosuccinimide (NHSS) in water was added onto GSH-AuNPs modified electrode for

10 min. After washing off these superfluous linkage reagents with water, 20 μL of 50 μg mL^{-1} of Ab_1 was added on the electrode and incubated at 36 °C for 3 h. The resulting surface was slowly washed with streams of 0.01 M pH 7.4 PBS containing 0.05% (w/v) Tween-20 and PBS to remove the physically absorbed Ab_1. The possible remaining active sites were blocked with 20 μL of 0.01 M pH 7.4 PBS containing 5% (w/v) bovine serum albumin (BSA) for 1 h at room temperature.

To carry out the immunoreaction and ECL measurements, the immunosensor was firstly incubated with 20 μL of CEA standard solution or serum sample for 30 min at 36 °C. After washing with PBST and PBS, it was further incubated with 20 μL of PFR-CdS QDs@PCNSs/Ab_2 for 90 min at 36 °C, followed by washing with PBST and PBS again. Finally, the ECL signal was detected in 0.1 M pH 9.0 PBS containing 0.1 M KNO_3.

Characterization

Photoluminescence (PL) and UV-vis absorption spectra were recorded on a RF-5301 PC fluorometer (Shimadzu Co., Japan) and a Shimadzu UV-3600 UV-Vis-NIR photospectrometer (Shimadzu Co., Japan), respectively. Attenuated total reflection (ATR)-FTIR spectra were recorded on a Vector 22 FTIR spectrometer (Bruker Optics, Germany). The time-resolved fluorescence spectra were collected with an Edinburgh FLS920 fluorescence spectrometer (Livingston, UK) by exciting the samples with an nF920 ultrafast nanosecond flashlamp at 440 nm and pulse width of about 0.8 ns with hydrogen filler gas. The temporal scanning range was selected as 120.0 ns with an instrument response function as fast as 0.25 ns. The specimens were also characterized by a JEM-2100 transmission electron microscope (TEM, Hitachi, Japan) with an accelerating voltage of 120 kV for low-resolution or 200 kV for high-resolution TEM images after drop-casting the sample dispersion onto a carbon-coated 300 mesh copper grid and dried under room temperature. The ζ potential was measured by a Nano-Z Zetasizer nanoparticle analyzer (Malvern Instruments Ltd, U.S.A). X-ray powder diffraction (XRD) patterns were recorded using a XRD-6000 diffractometer (Shimadzu Co., Japan), equipped with a rotating anode and a Cu Kα radiation source ($\lambda = 1.54178$ Å). Dynamic light scattering (DLS) measurement was performed by BI-200SM light scattering apparatus (Brookhaven, U.S.A.). Tapping mode atomic force microscopic (AFM) images of the samples cast on freshly cleaved mica sheets were acquired under ambient conditions using an Agilent 5500 AFM/SPM system (U.S.A.) and Picoscan v5.3.3 software. The reference levels of CEA in human serum samples were detected with an automated electrochemiluminescent analyzer (Elecsys 2010, Roche).

Electrochemiluminescence

ECL measurements were carried out on a MPI-E multifunctional electrochemical and chemiluminescent analytical system (Xi'an Remex Analytical Instrument Ltd. Co., China). A modified GCE (5 mm in diameter) as the working electrode, a platinum wire as the counter electrode and an Ag/AgCl (saturated KCl) as the reference electrode were used in all the electrochemical measurements, and all potentials were quoted against this reference electrode. Prior to modification, the GCE was polished to a mirror-like finish using 1.0 and 0.05 μm alumina slurry (Beuhler) followed by sonication in ethanol and water, rinsing with water and drying in an N_2 atmosphere. The QDs modified electrode for studying ECL behavior was prepared by casting 20 μL of 80 μM QDs aqueous solution on pretreated bare GCE at room temperature. The ECL cell was self-made with three side necks and one middle neck. The reference and counter electrodes were put in two side necks, while the electrode was put in the middle neck with its surface facing downward, approximating the optical window for recording the ECL signal. Another side neck was used for bubbling gas and injecting samples. The ECL emission window was placed in front of the photomultiplier tube (PMT, detection range from 300 to 650 nm) biased at −1000 V. Unless specially mentioned, the scan rate was 100 mV s^{-1}. The ECL spectra were obtained by collecting the intensity data at −0.80 V during cyclic potential sweep with 11 optical filters (2 mm thickness) with the transparent efficiency of around 88% at 650, 630, 600, 580, 550, 535, 510, 490, 470, 450 and 420 nm.

Results and discussion

The typical TEM image of PFR-CdS QDs showed a uniform size distribution of ~10 nm (Fig. 1A). This size approximated the mean hydrodynamic diameter of 11.2 nm evaluated from DLS analysis. The high-resolution TEM (HRTEM) image displayed magnified local crystalline zones that were indicative of a CdS lattice (Fig. 1B). This appearance distinguished CdS QDs from the amorphous polymer PFR as the stabilizer. In contrast, CdS QDs synthesized without PFR (Fig. 1C) emerged with an irregular geometry with large aggregates over 100 nm, indicating hydrothermal conditions improved bulk growth but greatly

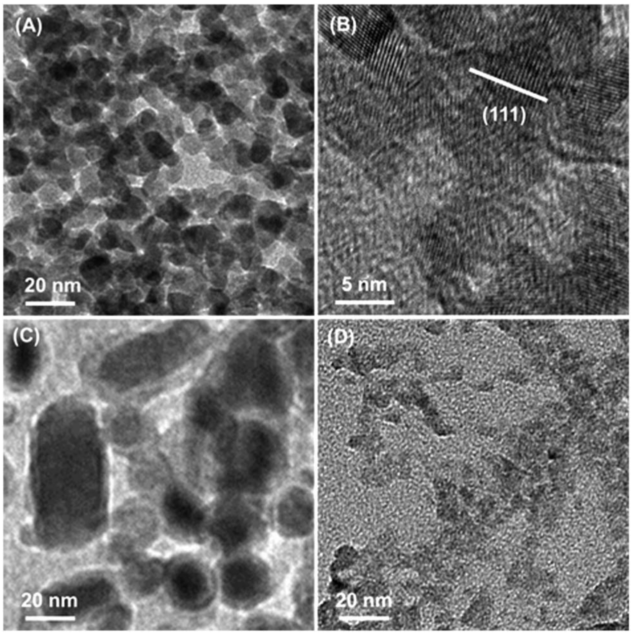

Fig. 1 (A) TEM and (B) HRTEM images of PFR-CdS QDs; TEM image of (C) CdS QDs and (D) MPA-CdS QDs.

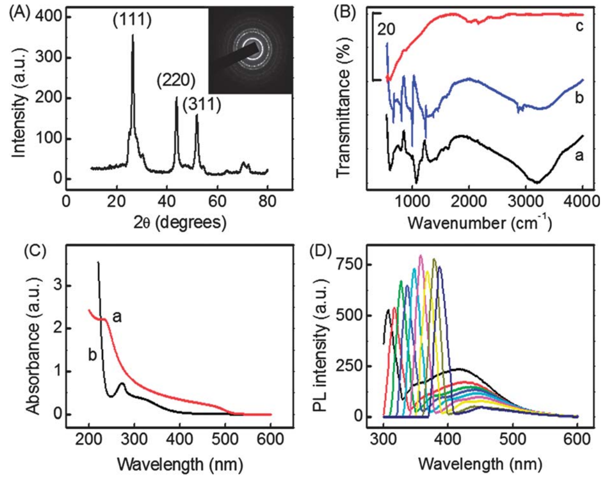

Fig. 2 (A) XRD pattern of PFR-CdS QDs. Inset: SAED pattern of PFR-CdS QDs. (B) ATR-FTIR spectra of (a) PFR-CdS QDs, (b) PFR and (c) MPA-CdS QDs. (C) UV-vis spectra of (a) PFR-CdS QDs and (b) PFR. (D) PL emission spectra of PFR ($\lambda_{ex} = 310$–390 nm, from left to right).

impacted the mono-dispersity and aqueous solubility. Thus the highly cross-linked PFR could be utilized to regulate the size of the QDs due to its polymeric conglutination effect.[18] As a control, CdS QDs capped with mercaptopropionic acid (MPA) were prepared according to the reported method[21] and revealed a relatively small size (<5 nm) (Fig. 1D).

The XRD pattern of PFR-CdS QDs exhibited three main peaks at scattering angles of 26.4°, 43.8° and 52.0° (Fig. 2A), corresponding to (111), (220) and (311) crystal planes with a blende structure (JCPDS card no.: 10-0454) and matching the polycrystalline concentric image from the selected area electron diffraction (SAED) (Fig. 2A, inset). Moreover, the crystal facet with the index [111] appeared as the most probable distribution in the XRD spectrum, indicating the nanocrystals observed in the HRTEM image mainly stacked along [111] direction. The ATR-FTIR spectrum showed the band positions of PFR-CdS QDs at 3350 cm^{-1} for the phenolic O–H stretch, 1168 and 1070 cm^{-1} for the alkyl-phenol C–O stretch and 902 cm^{-1} for the aromatic C–H in-plane deformation (Fig. 2B, curve a).[22] These peaks also occurred in the ATR-FTIR spectrum of PFR (Fig. 2B, curve b), while they were not observed in the CdS QDs (Fig. 2B, curve c), indicating a successful wrap of PFR on the QD surface. The slight shifts in band positions were possibly due to the attachment of PFR on the QDs.[23] The ζ potential of PFR-CdS QDs was measured to be −37.3 eV in water, suggesting high hydrophilicity for stable dispersion.

The UV-vis absorption spectrum of the PFR-CdS QDs showed two inflection points at 235 and 473 nm (Fig. 2C, curve a). The former belongs to the inherent optical absorption from the π-conjugation of the polymer (Fig. 2C, curve b), which blue-shifted from 270 nm of PFR to 235 nm of PFR-CdS QDs, demonstrating the decrease in the conjugation. Therefore, compared with the solid-nanoparticle morphology of the individual PRF,[23] PFR constituted the shell of PFR-CdS QDs. The size and concentration of the QDs solution were calculated to be 9.7 nm and 10.3 μM, respectively.[24]

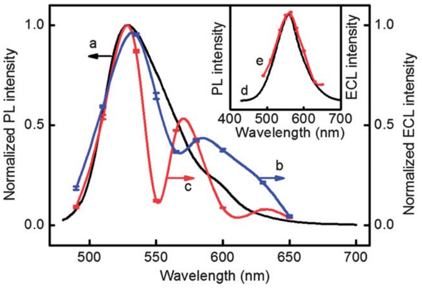

Fig. 3 (a) PL emission spectra of 80 μM PFR-CdS QDs in pH 8.0 PBS and ECL spectra of 80 μM PFR-CdS QDs in air-saturated (b) CH_2Cl_2 and (c) pH 8.0 PBS. Inset: (d) PL emission and (e) ECL spectra of 80 μM MPA-CdS QDs in air-saturated pH 8.0 PBS ($\lambda_{ex} = 440$ nm).

PFR showed an excitation-dependent photoluminescence (PL) behavior when the exciting wavelength (λ_{ex}) varied from 310 to 390 nm (Fig. 2D). On the contrary, the PL emission peak of the PFR-CdS QDs remained steady at around 537 nm (Fig. 3, curve a), illustrating the typical quantum confinement with the optimal λ_{ex} of 440 nm. These results confirmed that the PL emission originated from the core of the PFR-CdS QDs. The similar PL excitation and UV-vis absorption wavelengths indicated that the emitter was ascribed to the excited state (QD*), while the nonzero tail in the PL spectrum at longer wavelengths implied weak surface PL emission.[4]

ECL experiments further explored the internal relationship between PL and ECL emission (Fig. 3). The ECL spectra from PFR-CdS QDs in both organic and aqueous solutions revealed one main peak around 537 nm (Fig. 3, curves b and c), which was almost the same as the wavelength of the PL emission from the core (Fig. 3, curve a). However, the ECL spectra showed another strong broad peak at about 573 nm, which was also observed in the ECL spectrum of CdSe/ZnSe QDs.[4] This peak resulted from the surface traps of the passivated QDs, which corresponded to the nonsymmetric tail in the PL spectrum. This phenomenon was quite different from the sole core-typed ECL emission of MPA-CdS QDs (Fig. 3, inset). Moreover, the ECL emission from the surface traps was stronger in phosphate buffer solution (PBS) than that in CH_2Cl_2, suggesting a notable solvent effect on the surface states.

The PFR-CdS QDs modified glassy carbon electrode (GCE) produced an intensive ECL radiation with an emission peak at −0.78 V and an onset potential of −0.60 V in air-saturated pH 9.0 PBS (Fig. 4A, curve a). Here the ECL potential was the same as that of PFR-CdS QDs in aqueous solution and the dissolved O_2 was verified to be an endogenous coreactant of ECL emission (Fig. 4B, inset). The ECL peak potential shifted positively by 400 mV in comparison with the MPA-CdS QDs (Fig. 4A, curve b), 900 mV more positive than that of the similarly sized CdS QDs.[25] and was even more positive than the modified CdS QDs systems, such as the CdS QDs/carbon nanotube (CNT) hybrid (−1.22 V),[21] CdS QDs *in situ* anchored CNT (−1.05 V),[26] and the CdS QDs *in situ* decorated graphene nanocomposites (−1.13 V),[27] and CdS QDs/carbon nanosphere assembly (−1.15 V),[28] in which the modified CdS QDs could take refuge from the carbon nanomaterials to improve the ECL

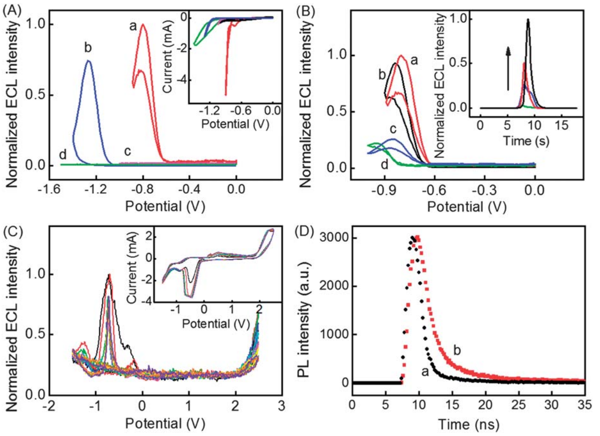

Fig. 4 (A) ECL responses of (a) PFR-CdS QDs, (b) MPA-CdS QDs, (c) uncapped CdS QDs and (d) PFR modified GCEs in air-saturated pH 8.0 PBS. Inset: corresponding CVs. (B) ECL responses of 80 μM PFR-CdS QDs prepared with (a) phenol and (b) *m*-cresol as the precursor in air-saturated pH 8.0 PBS and (a) in the PBS containing (c) 10 μM phenol and (d) HCHO. Inset: ECL responses of PFR-CdS QDs modified GCE in N_2-saturated, N_2-saturated with 320 μM H_2O_2, air-saturated and O_2-saturated (from bottom to top) pH 8.0 PBS. (C) Cyclic ECL curves of PFR-CdS QDs in air-free CH_2Cl_2 containing 0.1 M tetrabutylammonium perchlorate. Inset: corresponding CVs. (D) Time-resolved PL spectra ($\lambda_{ex} = 440$ nm) of (a) MPA-CdS QDs and (b) PFR-CdS QDs.

performance. The ECL of PFR-CdS QDs managed to avoid the problem of the so-called "blackbody effect" existing in the modified CdS QDs.[26,27] To the best of our knowledge, this is the lowest cathodic ECL peak potential in a QDs-based ECL system.[25–29] Furthermore, the PFR-CdS QDs showed a much stronger ECL emission than uncapped CdS QDs (Fig. 4A, curve c), as the uncapped CdS QDs inherently possessed relatively small specific areas and low aqueous solubility resulting from the unrestrained crystalline growth, which were unfavorable for the electron communication between QDs and the electrode, also disabled stable modification. In comparison among curves in Fig. 4A, this low-potential and intensive ECL emission resulted from the contribution of surface traps induced by PFR passivation, as the surface traps generally possess a narrower band gap compared with the core.[5]

The composition of PFR also affected the ECL emission. When using *m*-cresol to substitute phenol, the obtained methylated PFR-CdS QDs showed a more negative ECL potential and weaker ECL intensity (Fig. 4B, curves a and b), which was due to the σ–π hyperconjugation effect between methyl and phenyl. Interestingly, trace amounts of phenol and HCHO could greatly quench the ECL emission (Fig. 4B, curves c and d) through the energy transfer. Thus the purification of the QDs was very important.

The cathodic ECL curve of PFR-CdS QDs showed a "second" emission in the backward potential scan (Fig. 4A, curve a), where the cyclic voltammogram showed a crossover of the reduction current with the oxidation current (Fig. 4A, inset). Given the similar overlapping during the oxygen reduction reaction at metallic nanomaterial modified GCE,[30] intermediates with comparatively long lifetimes were assumed to exist. Meanwhile, the surface states of QDs could capture injected electrons, like holding them in metastable states, which was quite similar to the electron-holding behavior of *n*-type metallic oxide semiconductor, like anatase TiO_2.[31,32] From these points, PFR wrapping left QD distinctive surface states, which made their ECL behavior quite different from MPA-CdS QDs (Fig. 4A, curve b) as well as other reported QDs-based ECL phenomena.[4–10,25,29]

As the ECL signal is synchronously stimulated by electrochemistry, cyclic voltammetry (CV) was applied to investigate the intrinsic band parameters. The inset in Fig. 4C shows the typical CVs of PFR-CdS QDs in air-free dipolar aprotic solvent CH_2Cl_2. A prominent and broad cathodic peak at −0.48 V and an anodic peak at +2.28 V are observed with cathodic ECL peaking at −0.68 V, indicating the PFR-CdS QDs intrinsically possess a conduction band with low energy level, which facilitates the electron injection and the subsequent ECL emission at low potential. Furthermore, compared with the potential in air-saturated PBS, the peak potential in CH_2Cl_2 moved slightly from −0.78 to −0.68 V, which could be explained with the Nernstian equation, that the accumulated ratio of $[QD^+]/[QD^-]$ in the annihilation route draws the formal potential towards zero.[33,34] The potential difference of 2.76 V between −0.48 and +2.28 V is consistent with 2.62 eV calculated from the optical band gap in UV-vis spectrum (Fig. 2C, curve a). Meanwhile, both the anodic and cathodic peak intensities decreased at the initial two cycles and then stayed stable, which was consistent with the inset CV behavior, suggesting this annihilation accessed its equilibrium. Thus it was necessary to perform continuous cyclic scans for a stable ECL emission. The cathodic ECL intensity in Fig. 4C was larger than the anodic one, indicating the oxidized state (QD^+) was more stable than the reduced state (QD^-) and accumulated as the time elapsed.[35,36] In comparing this annihilation course with the coreactant one (Fig. 4A, curve a), the "crossover" in the cyclic voltammogram could be considered to be related with the solvent and the coreactant, which overall favored the formation of QD* for ECL emission.

Despite the difference in the stimulating source, ECL and PL shared similarities in the excited luminescence. In this way, time-resolved PL spectroscopy was further employed to deconstruct the exitonic luminescence and investigate the surface states by monitoring and comparing the excited lifetimes of MPA-CdS and PFR-CdS QDs. Both fluorescence decay curves were fitted into exponential functions in the form of $f = A + B_1\exp(-t/\tau_1) + B_2\exp(-t/\tau_2)$ with two decay components of τ_1 and τ_2, while B_1 and B_2 were their corresponding linear combination coefficients, reflecting the contribution of each component to the PL decay. As for MPA-CdS QDs, the analytical expression is $f_{MPA} = A_1 + 975.346e^{-t/0.8422} + 69.254e^{-t/5.5410}$; while $f_{PFR} = A_2 + 712.736e^{-t/2.2230} + 191.089e^{-t/14.9608}$ for PFR-CdS QDs. The fast components showed the time constants of 0.8 and 2.2 ns for MPA-CdS (Fig. 4D, curve a) and PFR-CdS QDs (Fig. 4D, curve b), while the slow ones showed the time constants of 5.5 and 15.0 ns, respectively. The τ_1 normally represents the excitonic lifetime, while τ_2 is attributed to the surface defects of QDs that trapped electrons at the conduction band to generate a new excited state (QDs*).[37] By evaluating the correlation of each component *via* calculating the fitting standard deviation of B_1 and B_2, τ_2 there emerged a relatively weak correlation (11.8%) for MPA-CdS QDs, while a major correlation (34.3%) for PFR-CdS QDs, which led to the long lifetime of the QDs*. The observed long-time constant was consistent with the ECL spectrum of PFR-CdS QDs.

In a word, the low-potential ECL emission of PFR-CdS QDs was derived from their unique surface states and intrinsic low conduction band, whereas the surface states elongated the excited lifetime of injected electrons during these cathodic low-potential ECL kinetics.

Several experimental parameters need to be optimized for obtaining the best ECL performance of QDs including the hydrothermal time, the ratio of phenol and HMTA, the amount of QDs for modification, the buffer electrolytes, the solution pH and the incubation time. As seen from Fig. 5A, with increasing hydrothermal duration, the ECL peak potential of PFR-CdS QD films shifted negatively, indicating the harder injection of electrons to the surface states of QD particles. Moreover, the ECL intensity decreased due to the relatively small surface-to-volume ratio of QDs, which decreased the contact area of the QDs with the electrode and the efficient electron transfer.[29] Since the QDs obtained with a hydrothermal duration of 5 h gave a sufficient, sensitive response and the lowest ECL peak potential, this time was selected for preparing the ECL emitter.

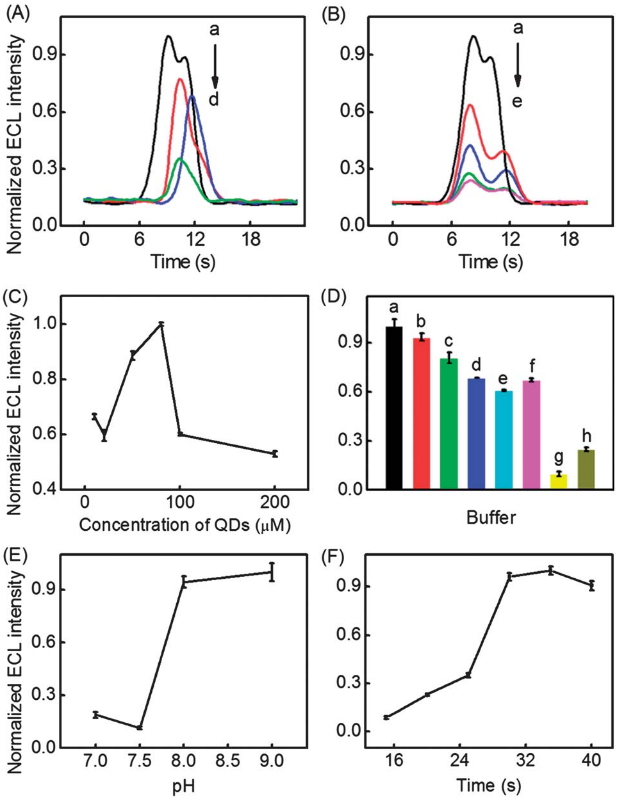

Fig. 5 Effects of (A) hydrothermal time and (B) monomer concentration on ECL intensity. (A) (a) 5, (b) 6, (c) 8 and (d) 10 h; (B) (a) 0.02 mmol phenol + 0.05 mmol HMTA, (b) 0.01 mmol phenol + 0.05 mmol HMTA, (c) 0.05 mmol phenol + 0.025 mmol HMTA, (d) 0.01 mmol phenol + 0.025 mmol HMTA, and (e) 0.005 mmol phenol + 0.025 mmol HMTA. Effects of (C) QDs concentration for modification, (D) buffer pH and electrolyte at (a) 9.0 and (b) 8.0 for PBS, (c) 9.0 and (d) 8.0 for BBS, (e) 10.0 and (f) 9.2 for CBS, and (g) 9.0 and (h) 8.0 for Tris, (E) pH of PBS on ECL intensity of PFR-CdS modified electrodes and (F) effect of incubation time for immunoassay of CEA on ECL intensity.

Since ammonia was a product from the pyrolysis of HMTA and TAA, it can be speculated that the concentration of NH_3 may be the main factor for the formation of the core–shell-structured QD. Due to the stability constant of 4.0×10^6 for $[Cd(NH_3)_4]^{2+}$, the increase in NH_3 could cause the initial growth of the CdS nucleus to be slower than that in the case without the capping agent. Furthermore, NH_3 has been reported to play a key role in the copolymerization of PFR.[17,18] Therefore, $[Cd(NH_3)_4]^{2+}$ constituted a temporary interface not only as the resulting surface of QD but for the formation of a polymerized shell, which further indicated that surplus HMTA could act as a coordinating and crosslinking agent. Thus with increasing the amount of HMTA from 0.025 to 0.05 mM, the ECL intensity of PFR-CdS QDs greatly increased (Fig. 5B), which further validated the contribution of the surface state to the ECL of PFR-CdS QDs. Meanwhile, the polymerization rate also counted on the concentration of phenol through restraining the size of QDs. Therefore, 0.02 mmol phenol and 0.05 mmol HMTA were the most appropriate amounts for copolymerization.

The quantity of the excited state (QD*) essentially depends on the amount of QDs. The strongest ECL intensity was obtained when 20 μL of 80 μM QDs solution was employed for modification (Fig. 5C), and more QDs led to a decrease in ECL response due to the inhibited electron exchange by the thicker semiconducting QDs film.

The cathodic ECL intensity of PFR-CdS QDs depended on the components and pH of the electrolytes. As shown in Fig. 5D, the ECL intensity of the resulting PFR-CdS QDs modified electrode in pH 9.0 PBS was higher than those in pH 9.0 and 8.0 borate buffer solution (BBS), pH 10.0 and 9.2 carbonate buffer solution (CBS) and much higher than those in pH 9.0 and 8.0 tris(hydroxymethyl)aminomethane (Tris)-HCl buffers. Meanwhile, the ECL intensity increased with the increasing pH of PBS from 7.0 to 9.0 and reached a plateau at 9.0 (Fig. 5E). Considering the bioactivity of immunoreagents, 8.0 PBS was selected for ECL measurement. Thus, 0.1 M pH 8.0 PBS was selected as the detection solution throughout the following experiments.

Incubation time is an important parameter in immunoassay. With increasing the incubation time up to 30 min, the ECL emission quickly increased due to the increasing amount of PFR-CdS QDs@CNSs/Ab_2 bound to the immunosensor surface, and thus generating the ECL emission (Fig. 5F). At the

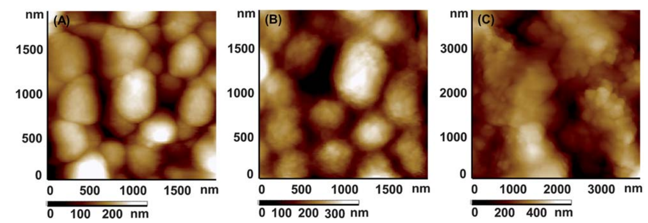

Fig. 6 AFM images of (A) CNSs, (B) PFR-CdS QDs@PCNSs and (C) PFR-CdS QDs@PCNSs/Ab_2.

incubation time of 30 min, the ECL emission tended to a maximum value, indicating a saturated binding among the captured antibody, analyte and the tracing tag. Therefore, 30 min of incubation time was chosen for the sandwich-type immunoassay.

Taking advantage of the low-potential and efficient ECL emission of PFR-CdS QDs, a facile "signal-on" strategy was proposed by immobilizing QDs on the carbon nanospheres (CNS) as the nanocarrier for signal amplification. Fig. 6 is the AFM characterization for preparation of the probe. The carboxylated CNSs with a uniform diameter around 200 nm (Fig. 6A) was firstly functionalized with PDDA and then PFR-CdS QDs through electrostatic adsorption, which led to the increasing diameter to 300 nm and rougher surface (Fig. 6B). The immobilization of antibody on the polymer-coated colloidal particles offered a facile access to the stable attachment of biomolecules while retaining their specific immunorecognition capability. Upon the immobilization of Ab_2 on the negative-charged PFR through electrostatic adsorption, an obvious agglomeration of the trapped biomolecules could be observed on the surface (Fig. 6C).

As shown in Fig. 7, the ECL intensity increased with increasing CEA concentration in incubation solution under the optimal synthetic and detection conditions with dissolved oxygen as the endogenous coreactant, which was attributed to the increasing amount of PFR-CdS QDs@PCNSs/Ab_2 to form the sandwich immunocomplex. The ECL peak potential of −1.22 V different from −0.78 V at PFR-CdS QDs modified GCE was due to the steric hindrance from the sandwich format. The calibration plot showed a good linear relationship between the ECL intensity and the logarithm value of CEA concentration ranging from 10 ng mL^{-1} to 1 pg mL^{-1} with a correlation coefficient of 0.996 (Fig. 7, inset). The detection limit at a signal-to-noise ratio of 3 was 0.83 pg mL^{-1}, which was lower than 1.4 pg mL^{-1} by dual signal amplification of glucose oxidase-functionalized nanocomposites as a trace label for electrochemical immunoassay[38] and 1.6 pg mL^{-1} by chemiluminescence imaging immunoassay.[39] More importantly, this immunoassay showed a wide detection range of 6 orders of magnitude and avoided the need for deoxygenation in general electrochemical immunoassay.

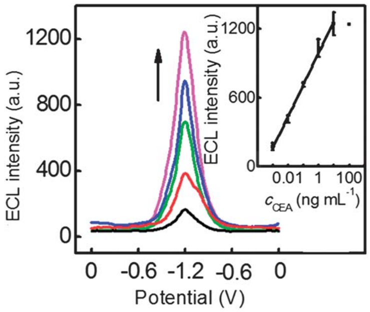

Fig. 7 ECL responses of the fabricated immunosensor to CEA at 1 pg mL^{-1}, 10 pg mL^{-1}, 100 pg mL^{-1}, 1 ng mL^{-1} and 10 ng mL^{-1} (from bottom to top). Inset: calibration curve.

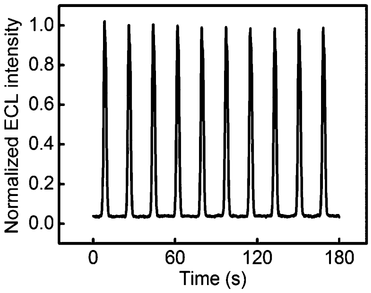

Fig. 8 Continuous cyclic scans of the immunosensor in air-saturated detection solution after incubation with 5 ng mL^{-1} of CEA and then the labeled tracing tag PFR-CdS QDs@PCNSs/Ab_2.

Table 1 Assay results of CEA (ng mL^{-1}) in clinical serum samples using the proposed and reference methods

Sample no.	1	2	3
Proposed method	1.35	3.40	4.94
Reference method	1.29	3.17	5.32
Relative error (%)	−4.65	−7.26	7.14

Both the intra-assay and inter-assay precisions of the ECL immunosensor were examined at 5 ng mL^{-1} CEA seven times. The relative standard deviations (RSD) were 8.8% and 11.2%, respectively, showing the good precision and acceptable fabrication reproducibility. Nine measurements of ECL emission upon continuous cyclic scans of the ECL immunosensor for 5 ng mL^{-1} CEA showed coincident signal with RSD of 1.14% (Fig. 8), indicating acceptable reliability and stability of the detection signal.

The analytical reliability and application potential of the proposed method were evaluated by comparing the assay results of clinical serum samples with the reference values from commercial ECL single-analyte tests (Table 1), indicating acceptable accuracy of the proposed method for the detection of CEA in clinical samples.[40]

Conclusions

This work presented a novel method for the synthesis of polymer-stabilized quantum dots (QDs) to produce surface-state controlled ECL emission. The PFR polymer could be formed *in situ* to passivate the surface of the QDs, which led to a uniform size distribution and controllable surface states. The ECL spectrum showed two peaks corresponding to the core and surface states of QDs. The strong surface-state controlled ECL emission occurred at a relatively low potential with elongated lifetime. A new signal tag was designed for taking advantage of the surface-state controlled ECL in a "signal-on" ECL immunoassay. The developed sandwich-typed immunoassay method showed a linear range over 5 orders of magnitude with high sensitivity. The functionalized QDs could be conveniently used to label other biorecognition elements, showing the promising application of the surface passivated PFR-capped QDs in optoelectronic and biomedical devices.

Acknowledgements

This work was financially supported by the National Basic Research Program of China (2010CB732400) and the National Natural Science Foundation of China (21121091, 21135002).

References

1 L. F. Sun, L. Bao, B. R. Hyun, A. C. Bartnik, Y. W. Zhong, J. C. Reed, D. W. Pang, H. D. Abruña, G. G. Malliaras and F. W. Wise, *Nano Lett.*, 2009, **9**, 789.
2 W. J. Miao, *Chem. Rev.*, 2008, **108**, 2506.
3 R. Gill, M. Zayats and I. Willner, *Angew. Chem., Int. Ed.*, 2008, **47**, 7602.
4 N. S. Myung, Y. J. Bae and A. J. Bard, *Nano Lett.*, 2003, **3**, 1053.
5 Y. J. Bae, N. S. Myung and A. J. Bard, *Nano Lett.*, 2004, **4**, 1153.
6 S. K. Haram, B. M. Quinn and A. J. Bard, *J. Am. Chem. Soc.*, 2001, **123**, 8860.
7 S. K. Poznyak, D. V. Talapin, E. V. Shevchenko and H. Weller, *Nano Lett.*, 2004, **4**, 693.
8 G. D. Liang, L. P. Shen, G. Z. Zou and X. L. Zhang, *Chem.–Eur. J.*, 2011, **17**, 10213.
9 S. N. Ding, B. H. Gao, D. Shan, Y. M. Sun and S. Cosnier, *Chem.–Eur. J.*, 2012, **18**, 1595.
10 Y. M. Fang, J. Song, R. J. Zheng, Y. M. Zeng and J. J. Sun, *J. Phys. Chem. C*, 2011, **115**, 9117.
11 H. X. Ju, X. J. Zhang and J. Wang, *NanoBiosensing – Principles, Development and Applications*, Springer, New York, 2011.
12 T. Hu, T. S. Li, L. Yuan, S. Q. Liu and Z. L. Wang, *Nanoscale*, 2012, **4**, 5447.
13 N. Gaponik and A. L. Rogach, *Phys. Chem. Chem. Phys.*, 2010, **12**, 8685.
14 X. Liu, L. X. Cheng, J. P. Lei, H. Liu and H. X. Ju, *Chem.–Eur. J.*, 2010, **16**, 10764.
15 Y. Liu, R. Brandon, M. Cate, X. G. Peng, R. Stony and M. Johnson, *Anal. Chem.*, 2007, **79**, 8796.
16 M. S. Nikolic, M. Krack, V. Aleksandrovic, A. Kornowski, S. Förster and H. Weller, *Angew. Chem., Int. Ed.*, 2006, **45**, 6577.
17 A. H. Lu, G. P. Hao and Q. Sun, *Angew. Chem., Int. Ed.*, 2011, **39**, 9023.
18 A. H. Lu, W. C. Li, G. P. Hao, B. Spliethoff, H. J. Bongard, B. B. Schaack and F. Schüth, *Angew. Chem.*, 2010, **122**, 1659.
19 X. M. Sun and Y. D. Li, *Angew. Chem., Int. Ed.*, 2004, **43**, 597.
20 X. Yu, B. Munge, V. Patel, G. Jensen, A. Bhirde, J. D. Gong, S. N. Kim, J. Gillespie, J. S. Gutkind, F. Papadimitrakopoulos and J. F. Rusling, *J. Am. Chem. Soc.*, 2006, **128**, 11199.
21 S. N. Ding, J. J. Xu and H. Y. Chen, *Chem. Commun.*, 2006, 3631.
22 P. Yang, Y. Zhao, Y. Lu, Q. Z. Xu, X. W. Xu, L. Dong and S. H. Yu, *ACS Nano*, 2011, **5**, 2147.
23 S. R. Guo, J. Y. Gong, P. Jiang, M. Wu, Y. Lu and S. H. Yu, *Adv. Funct. Mater.*, 2008, **18**, 872.
24 W. W. Yu, L. H. Qu, W. Z. Guo and X. G. Peng, *Chem. Mater.*, 2003, **15**, 2854.
25 G. F. Jie, B. Liu, H. C. Pan, J. J. Zhu and H. Y. Chen, *Anal. Chem.*, 2007, **79**, 5574.
26 X. F. Wang, Y. Zhou, J. J. Xu and H. Y. Chen, *Adv. Funct. Mater.*, 2009, **19**, 1.
27 K. Wang, Q. Liu, X. Y. Wu, Q. M. Guan and H. N. Li, *Talanta*, 2010, **82**, 372.
28 Y. Y. Zhang, S. Y. Deng, J. P. Lei, Q. N. Xu and H. X. Ju, *Talanta*, 2011, **85**, 2154.
29 L. X. Cheng, X. Liu, J. P. Lei and H. X. Ju, *Anal. Chem.*, 2010, **82**, 3359.
30 B. Yue, Y. W. Ma, H. S. Tao, L. S. Yu, G. Q. Jian, X. Z. Wang, X. S. Wang, Y. N. Lu and Z. Hu, *J. Mater. Chem.*, 2008, **18**, 1.
31 K. Kawahara, K. Suzuki, Y. Ohko and T. Tatsuma, *Phys. Chem. Chem. Phys.*, 2005, **7**, 3851.
32 I. Robel, M. Kuno and P. V. Kamat, *J. Am. Chem. Soc.*, 2007, **129**, 4136.
33 G. Z. Zou and H. X. Ju, *Anal. Chem.*, 2004, **76**, 6871.
34 C. W. Ge, M. Xu, J. Liu, J. P. Lei and H. X. Ju, *Chem. Commun.*, 2008, 450.
35 S. N. Inamdar, P. P. Ingole and S. K. Haram, *ChemPhysChem*, 2008, **9**, 2574.
36 S. K. Haram, A. Kshirsagar, Y. D. Gujarathi, P. P. Ingole, O. A. Nene, G. B. Markad and S. P. Nanavati, *J. Phys. Chem. C*, 2011, **115**, 6243.
37 A. N. Cao, Z. Liu, S. S. Chu, M. H. Wu, Z. M. Ye, Z. W. Cai, Y. L. Chang, S. F. Wang, Q. H. Gong and Y. F. Liu, *Adv. Mater.*, 2009, **21**, 1.
38 G. S. Lai, F. Yan and H. X. Ju, *Anal. Chem.*, 2009, **81**, 9730.
39 C. Zong, J. Wu, C. Wang, H. X. Ju and F. Yan, *Anal. Chem.*, 2012, **84**, 2410.
40 S. Ishigami, S. Natsugoe, S. Hokita, X. M. Che, K. Tokuda, A. Nakajo and H. Iwashige, *J. Clin. Gastroenterol.*, 2001, **1**, 41.